ELSEVIER

Biophysical Chemistry 117 (2005) 27 – 37

Biophysical Chemistry

http://www.elsevier.com/locate/biophyschem

# Core–shell nanocluster films of hemoglobin and clay nanoparticle: Direct electrochemistry and electrocatalysis

Yi Liu, Hongyun Liu, Naifei Hu*

*Department of Chemistry, Beijing Normal University, Beijing 100875, China*

Received 31 January 2005; received in revised form 27 April 2005; accepted 27 April 2005
Available online 17 May 2005

**Abstract**

A novel core–shell protein nanocluster film, designated as clay–$(Hb/PSS)_n$, was fabricated on pyrolytic graphite (PG) electrodes. Positively charged hemoglobin (Hb) at pH 5.5 and negatively charged poly(styrenesulfonate) (PSS) were first assembled layer by layer on surface of clay nanoparticles from their solutions mainly by electrostatic attraction, forming a core–shell nanocluster structure in which clay nanoparticles were the "cores" and $(Hb/PSS)_n$ multilayers were the "shells". The aqueous dispersion of clay–$(Hb/PSS)_n$ nanoclusters was then cast on surface of PG electrodes, forming clay–$(Hb/PSS)_n$ nanocluster films after evaporation of solvent. Hb in clay–$(Hb/PSS)_n$ films exhibited a pair of well-defined and reversible cyclic voltammetric (CV) peaks at about −0.36 V vs. SCE in pH 7.0 buffers, characteristic of Hb heme Fe(III)/Fe(II) redox couples. Compared with other Hb-containing clay films, clay–$(Hb/PSS)_n$ films displayed smaller CV peak separation ($\Delta E_p$), indicating the better electrochemical reversibility of Hb in these nanocluster films. The partially ordered structure of the films was characterized by X-ray diffraction (XRD) experiments. UV–VIS and reflection absorption infrared (RAIR) spectroscopy suggests that Hb retains its near-native structure in clay–$(Hb/PSS)_n$ films. Oxygen, hydrogen peroxide, and nitrite were catalytically reduced at clay–$(Hb/PSS)_n$ film electrodes, showing the potential applicability of the films as the new type of biosensors or bioreactors based on protein direct electrochemistry. The electrochemical and electrocatalytic activity of the films could be tailored by controlling the number of bilayers of the $(Hb/PSS)_n$ shells on the surface of clay nanoparticle cores.


*Keywords:* Hemoglobin; Clay; Core–shell nanocluster; Direct electrochemistry; Electrocatalysis

## 1. Introduction

Since 1990s, the direct electrochemistry of redox proteins in thin films modified on electrode surface has aroused increasing interest among researchers for their theoretical significance and perspective application in electrochemical biosensors and bioreactors [1–4]. The thin films may provide a suitable microenvironment for the proteins and enhance the direct electron transfer between the proteins and underlying electrodes [5,6]. Recently, layer-by-layer assembly based on alternate adsorption of oppositely charged polyions from their solutions has also been used to build up ultrathin protein films [7,8]. One of the advantages of layer-by-layer assembly over the cast method is the precise control of film composition and thickness at molecular level or in nanometer size. The direct electrochemistry of proteins in layer-by-layer films has also been studied. For example, Lvov et al. [9] constructed layer-by-layer films of myoglobin (Mb) or cytochrome $P450_{cam}$ (Cyt P450) with oppositely charged DNA or poly(styrenesulfonate) (PSS) on gold electrodes. Reversible cyclic voltammograms of Mb and Cyt P450 in these films were achieved. We reported the assembly of layer-by-layer films of heme proteins with various polyions or nanoparticles on pyrolytic graphite (PG) electrodes [10–16]. Direct and reversible voltammograms of the proteins

* Corresponding author.
*E-mail address:* hunaifei@bnu.edu.cn (N. Hu).

0301-4622/$ - see front matter © 2005 Elsevier B.V. All rights reserved.
doi:10.1016/j.bpc.2005.04.010

in these films were observed and used to electrocatalyze various substrates. The protein layer-by-layer films assembled on planar solid supports have also been extended to curved surfaces of submicrometer-sized particles or nanometer-sized colloids [17–19], forming "core–shell" clusters where the small particles are "cores" and the multibilayer {protein/polyion}$_n$ films assembled on the core surface are "shells". In our laboratory, the core–shell clusters with heme protein shells assembled on polystyrene latex or silica nanoparticle cores were further cast or assembled layer by layer on PG electrodes [20–22], and the direct electrochemistry of the proteins in these films was realized. The electrochemical and electrocatalytic activity of the proteins in these core–shell cluster films could be tailored by controlling the number of bilayers of the shells.

Clays are stable aluminosilicates with high cation-exchange capacity, and exfoliated clay particles have a platelet shape with nanoscopic size [23]. Compared with organic polyelectrolytes, clay has the advantages of high chemical stability, good adsorption property due to its appreciable surface area, special structural feature, and unusual intercalation property. The interaction of proteins with clay has been studied extensively, and the direct electrochemistry of redox proteins such as hemoglobin (Hb), cytochrome *c* (Cyt *c*), horseradish peroxidase (HRP), and Mb in clay-related films has also been reported [24–34]. For example, our group has studied the electrochemical and electrocatalytic properties of heme proteins in cast protein–clay films and layer-by-layer {clay/proteins}$_n$ films modified on PG electrodes [32–34].

In the present work, the strategy of construction of the protein core–shell nanocluster films was extended to clay nanoparticles, and this new kind of clay films was used to immobilize Hb and realize its direct electrochemistry. Oppositely charged hemoglobin (Hb) and PSS were first assembled layer by layer on the surface of clay nanoparticles, forming core–shell clay–(Hb/PSS)$_n$ nanoclusters. The nanoclusters were then cast on PG electrodes, forming clay–(Hb/PSS)$_n$ films. The construction of the clay–(Hb/PSS)$_n$ nanoclusters and the clay–(Hb/PSS)$_n$ films were characterized by UV–VIS spectroscopy, cyclic and square wave voltammetry, X-ray diffraction (XRD), scanning electron microscopy (SEM), and reflection absorption infrared spectroscopy (RAIR). The feasibility of the protein films in electrochemical catalysis toward various substrates of biological or environmental significance was also studied. To the best of our knowledge, while the direct electrochemistry of Hb in different types of clay films was reported previously, the direct electrochemistry of Hb in this new type of core–shell nanocluster films concerning clay nanoparticles has not been studied until now. We expected that Hb in clay–(Hb/PSS)$_n$ films would demonstrate some unique and better properties in voltammetry and electrocatalysis than in other Hb-containing clay films.

## 2. Materials and methods

### 2.1. Reagents

Bovine hemoglobin (Hb, MW 67,000), bovine liver catalase (MW 240,000) and hemin (MW 651.96) were all from Sigma and used as received. Poly(sodium styrenesulfonate) (PSS, MW ~ 70,000) was from Aldrich. Montmorillonite clay was obtained from Source Clay Minerals Repository. Hydrogen peroxide ($H_2O_2$, 30%) was from Beijing Chemical Plant, and sodium nitrite ($NaNO_2$) was from Beijing Shuanghuan Chemical Reagent. Both $H_2O_2$ and $NaNO_2$ were freshly prepared before being used. All other chemicals were reagent grade.

Buffers were 0.05 M citric acid, 0.1 M sodium acetate, 0.05 M sodium dihydrogen phosphate, or 0.05 M boric acid, all containing 0.1 M KBr. Buffer pH was adjusted with HCl or KOH solutions. All solutions were prepared with twice-distilled water. Experiments were carried out at room temperature (20 ± 2 °C).

### 2.2. Pretreatment of clay

Before being used, clay was pretreated in the similar way as described in literature [35]. In brief, 5 g of clay was suspended in 100 mL of 1 M NaCl solution with energetic stirring for at least 48 h. The slurry was then centrifuged at 3000 rpm for 40 min. After the supernatant was discarded, 50 mL of pure water was added into the clay precipitation. After moderate stirring for 40 min, the clay colloid was centrifuged, and the supernatant containing smaller clay particles was collected. Another 50 mL of pure water was added into the remaining clay sediment, stirred for 40 min, and centrifuged again. This cycle was repeated several times and all supernatants were collected. The supernatant was then dialyzed in pure water until no $Cl^-$ was detected with $AgNO_3$. After the supernatant was vacuum lyophilized, the solid clay precipitation was obtained. Transmission electron microscopy (TEM) showed that most of the clay particles took a round platelet shape with diameter in the range of 50–70 nm with average 60 nm, indicating that the clay particles obtained by this pretreatment were nanometer-sized.

### 2.3. Assembly of clay–(Hb/PSS)$_n$ core–shell nanoclusters

Clay–(Hb/PSS)$_n$ nanoclusters were assembled with two main steps. In the first step, 2 mL of aqueous dispersions of clay (3 mg mL$^{-1}$, pH 5.5) were mixed with 2 mL of Hb solution (3 mg mL$^{-1}$) at pH 5.5 in a centrifuge tube for 25 min with occasional shaking so that Hb could be adsorbed on the surface of clay nanoparticles. The mixture was then centrifuged at 6000 rpm for 6 min to separate the Hb-coated clay nanoparticles from the supernatant. After the supernatant was discarded, the clay–Hb particles were redispersed in 4 mL of pH 5.5 buffers for washing. The dispersion was

then centrifuged again, and the supernatant was discarded. This redispersion/centrifugation cycle was repeated two additional times to ensure removal of all unadsorbed Hb from clay–Hb particles. In the second step, 2 mL of PSS solution (3 mg $mL^{-1}$) was added into the tube containing clay–Hb particles, and was mixed for 25 min. The PSS was then adsorbed onto the surface of the clay–Hb particles. After several washing cycles, the clay–(Hb/PSS) core–shell nanoclusters were collected. These two steps were repeated several times until the desired number of shell bilayers ($n$) was reached. In the present work, core–shell nanoclusters of clay–(Hb/PSS) with $n=1$ and clay–$(Hb/PSS)_2$ with $n=2$ were assembled, respectively, and their dispersions in pH 5.5 buffers were stored at 4 °C for further use.

### 2.4. Preparation of clay–$(Hb/PSS)_n$ films on electrodes

Prior to coating, basal plane pyrolytic graphite (PG, Advanced Ceramics, geometric area 0.16 $cm^2$) disk electrodes were polished freshly with metallographic sandpapers while flushing with water, ultrasonicated in water for 30 s, and then dried in air. Ten microliters of clay–$(Hb/PSS)_n$ dispersions were cast onto the surface of PG electrodes. A small bottle was fit tightly over the electrode so that water could be evaporated slowly and more uniform films were formed. After about 12 h of drying, the clay–$(Hb/PSS)_n$ films were further dried overnight in air.

### 2.5. Instruments and procedures

A CHI 660A electrochemical analyzer (CH Instruments) was used for cyclic and square wave voltammetry. In electrochemical measurements, a regular three-electrode cell was used with a saturated calomel electrode (SCE) as the reference, a platinum wire as the counter electrode, and a PG disk electrode coated with films as the working electrode. Voltammetry at clay–$(Hb/PSS)_n$ film electrodes was performed in buffers containing no Hb. Prior to measurements, buffer solutions were purged with purified nitrogen for at least 15 min, and then the nitrogen was bubbled gently through the solutions for exclusion of oxygen during the whole experiment. In aerobic experiments, measured volumes of air were injected into solutions via a syringe in a sealed cell, which had been previously degassed with nitrogen.

UV–VIS absorption spectroscopy was measured with a Cintra-10e UV–VIS spectrometer (GBC). Sample films for spectroscopy were prepared by depositing clay–$(Hb/PSS)_n$ dispersions onto quartz slides and drying in air. Reflection absorption infrared (RAIR) spectra of the films were obtained by a Vatar 360 FT-IR (Nicolet) spectrometer with a DTGS detector at 4 $cm^{-1}$ resolution. Films were prepared by depositing clay–$(Hb/PSS)_n$ dispersions onto aluminum disks. Transmission electron microscopy (TEM) image was taken with an H 600 TEM instrument (Hitachi) operating at 100 kV. X-ray diffraction (XRD) was done for films on glass slides with a D/MAX-RB powder diffractometer (Rigaku) using a Cu Kα source at 40 kV and 120 mA with scan rate of 1° $min^{-1}$. Scanning electron microscopy (SEM) was run with an X-650 scanning electron microanalyzer (Hitachi) at an acceleration voltage of 20 kV. Prior to SEM analysis, the films were coated with about 10 nm of Au by an IB-3 ion coater (Eiko).

## 3. Results and discussion

### 3.1. Assembly of clay–$(Hb/PSS)_n$ nanoclusters

With its isoelectric point at pH 7.4 [36], Hb is positively charged at pH 5.5. Thus, Hb was adsorbed on the surface of negatively charged clay platelets mainly by electrostatic interaction. Polyanionic PSS was then adsorbed on the surface of clay–Hb, forming a core–shell clay–(Hb/PSS) structure. This layer-by-layer assembly procedure was repeated several cycles to construct clay–$(Hb/PSS)_n$ nanoclusters. The growth of $(Hb/PSS)_n$ shells on the surface of clay cores was followed indirectly by UV–VIS spectroscopy. Taking adsorption of the first Hb layer on the clay particles as an example, the sensitive Soret adsorption band of Hb at 405 nm was measured for the initial protein solution at pH 5.5 before it was mixed with clay colloids. After the adsorption of Hb on clay surface was saturated, the Soret band of Hb was measured again for the supernatant. In the following washing steps, UV–VIS spectroscopic measurements were conducted for the supernatants. The results showed that after 3 cycles of redispersion/centrifugation steps, the amount of free or unadsorbed Hb in the supernatant was very limited and the Soret band could not be detected by UV–VIS spectroscopy. Ignoring the loss of clay nanoparticles in the whole adsorption process, the ratio of adsorbed Hb on clay surface over the total Hb in the initial adsorbate solution was estimated to be 49% for the first bilayer adsorption and 38% for the second bilayer adsorption by subtracting the Soret peak absorbance of several supernatants from the initial absorbance of Hb with volume adjustment. The amount of adsorbed Hb on the clay surface was approximately 0.40 (mg Hb/mg clay) for the clay–(Hb/PSS) nanoclusters and 0.70 (mg Hb/mg clay) for the clay–$(Hb/PSS)_2$ nanoclusters. The adsorbed Hb on the clay surface was very stable and could withstand several cycles of water washing, suggesting that the interaction between the protein and oppositely charged clay is quite strong.

### 3.2. Voltammetric behaviors

The electrochemical properties of clay–$(Hb/PSS)_n$ films on PG electrodes were studied by cyclic voltammetry (CV). While the clay–$(Hb/PSS)_n$ nanoclusters were assembled at pH 5.5 by electrostatic attraction between Hb and clay, the CV experiments of the clay–$(Hb/PSS)_n$ film electrodes were

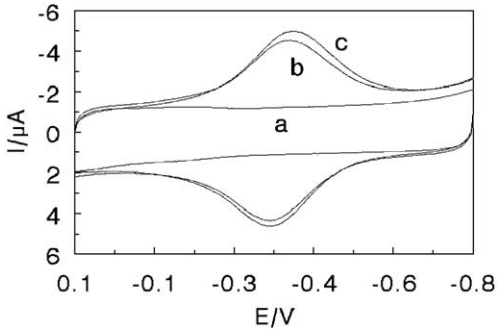


Fig. 1. Cyclic voltammograms at 0.2 V $s^{-1}$ in pH 7.0 buffers for (a) clay, (b) clay–(Hb/PSS), and (c) clay–$(Hb/PSS)_2$ films.

carried out at pH 7.0 which was closer to the biophysical condition of living systems. When clay–$(Hb/PSS)_n$ films were placed in Hb-free pH 7.0 buffers, a pair of well-defined, quasi-reversible CV peaks was observed at about −0.36 V vs. SCE (Fig. 1b and c). The peaks were located at the potential characteristic of the Hb Fe(III)/Fe(II) redox couples [37]. No CV peak was observed at clay-modified PG electrodes in the same potential range (Fig. 1a). This indicates the direct electron transfer between Hb and underlying PG electrodes in the clay–$(Hb/PSS)_n$ film system. The electron communication was much faster for clay–$(Hb/PSS)_n$ films than that for Hb in solution on bare PG. The core–shell nanocluster clay–$(Hb/PSS)_n$ films thus provide a favorable microenvironment for Hb to transfer electrons with underlying PG electrodes and have a great enhancement on the electron-transfer rates. Compared with clay–(Hb/PSS) films with $n=1$, clay–$(Hb/PSS)_2$ films with $n=2$ showed very similar peak positions and just slightly increased peak currents, suggesting that one more bilayer of Hb/PSS on the clay surface essentially does not increase the amount of electroactive Hb in the films. The CV parameters for clay–$(Hb/PSS)_n$ films and other Hb-containing clay films are listed in Table 1 for comparison.

CVs of clay–$(Hb/PSS)_n$ films had roughly symmetric peak shapes and nearly equal heights of reduction and oxidation peaks (Fig. 1). Both reduction and oxidation peak currents increased linearly with scan rates from 0.05 to 5 V $s^{-1}$. Integration of the reduction peaks gave nearly constant charge ($Q$) values independent of scan rates in the same scan rate range. All these results are characteristic of surface-confined or thin-layer electrochemical behavior [38], in which all electroactive HbFe(III) in the films are reduced to HbFe(II) on the forward cathodic scan, and the produced HbFe(II) are fully converted back to HbFe(III) form on the reverse anodic scan. Thus, the surface concentration of electroactive Hb ($\Gamma^*$, mol $cm^{-2}$) was estimated by integration of reduction peak of clay–$(Hb/PSS)_n$ films and using the equation of $Q=nFA\Gamma^*$ [39], where $A$ is the geometric area of PG electrode (0.16 $cm^2$), and $n$ and $F$ have their usual meanings. In the range of scan rate from 0.05 to 5 V $s^{-1}$, the average $\Gamma^*$ value was $7.34\times10^{-11}$ mol $cm^{-2}$ for clay–(Hb/PSS) films and $8.30\times10^{-11}$ mol $cm^{-2}$ for clay–$(Hb/PSS)_2$ films. According to the amount of Hb adsorbed on the clay nanoparticles estimated by UV–VIS spectroscopy and the deposition amount of clay–$(Hb/PSS)_n$ nanoclusters on PG, the surface concentration of total deposited Hb ($\Gamma$, mol $cm^{-2}$) on the PG surface was estimated to be $8.87\times10^{-10}$ mol $cm^{-2}$ for clay–(Hb/PSS) films and $1.58\times10^{-9}$ mol $cm^{-2}$ for clay–$(Hb/PSS)_2$ films. Thus, the fraction of electroactive Hb among the total adsorbed Hb in clay–$(Hb/PSS)_n$ films ($\Gamma^*/\Gamma$) was around 8.3% at $n=1$ and 5.3% at $n=2$ (Table 1).

Square wave voltammetry (SWV) has better signal-to-noise ratio and resolution than CV [40] and is easier to be analyzed quantitatively. SWV, combined with nonlinear regression, was thus used to estimate the apparent heterogeneous electron transfer rate constant ($k_s$) and formal potential ($E^{\circ\prime}$) of clay–$(Hb/PSS)_n$ films. The working model was a combination of the single-species surface-confined SWV model [41] and the formal potential dispersion model, as described in detail previously [42,43]. The SWV data for clay–$(Hb/PSS)_n$ films showed accuracy of fit on the model over a range of amplitudes and frequencies (data not shown). The average $k_s$ and $E^{\circ\prime}$ values obtained by this method at pH 7.0 for clay–$(Hb/PSS)_n$ films are also listed in Table 1. Both clay–(Hb/PSS) and clay–$(Hb/PSS)_2$ films showed relatively large $k_s$ values, consistent with the well-defined and quasi-reversible CV responses of the films, indicating that the nanocluster films

Table 1
Electrochemical parameters of Hb-containing clay films at pH 7.0

| Films[a] | $E^{\circ\prime}/V$ vs. SCE | | $\Delta E_p$/(mV) | $\Gamma$/(mol $cm^{-2}$) | $\Gamma^*$/(mol $cm^{-2}$) | $\Gamma^*/\Gamma$ | $k_s/(s^{-1})$ | Ref.[b] |
|---|---|---|---|---|---|---|---|---|
| | CV | SWV | | | | | | |
| Clay–(Hb/PSS) | −0.363 | −0.367 | 34 | $8.87\times10^{-10}$ | $7.34\times10^{-11}$ | 8.3% | 41±3 | tw |
| Clay–$(Hb/PSS)_2$ | −0.355 | −0.360 | 44 | $1.58\times10^{-9}$ | $8.30\times10^{-11}$ | 5.3% | 36±4 | tw |
| Hb–clay | −0.348 | −0.361 | 65 | $5.31\times10^{-10}$ | $6.3\times10^{-11}$ | 11.9% | 31±2 | [32] |
| $\{Clay/Hb\}_6$ | −0.322 | −0.340 | 87 | $8.10\times10^{-10}$ | $1.77\times10^{-10}$ | 21.8% | 42±3 | [34] |
| Hb/clay/GCE | −0.391 | | 140 | | | | 79 | [25] |
| Hb-mont | −0.373 | | 100 | | | | | [24] |

[a] GCE=glassy carbon electrode, mont=sodium montmorillonite.
[b] tw: this work, reporting $E^{\circ\prime}$ and $\Delta E_p$ values from CV at 0.2 V $s^{-1}$ or average values of $E^{\circ\prime}$ and $k_s$ from analysis of eight SWVs at frequencies of 100–175 Hz, amplitudes of 60–75 mV, and a step height of 4 mV.

provide a favorable microenvironment for Hb and enhance the rate of electron transfer between Hb and underlying PG electrodes. The $E^{o\prime}$ value estimated by SWV was in good agreement with that obtained by CV for the same films.

While the clay–(Hb/PSS)$_n$ films showed the $k_s$ value in the same order of magnitude as that of cast Hb–clay and layer-by-layer {clay/Hb}$_6$ films, the nanocluster films demonstrated smaller peak separation ($\Delta E_p$) than other Hb-containing clay films (Table 1). This indicates that the electrochemical reversibility of Hb in the clay–(Hb/PSS)$_n$ films is greatly improved. Although the exact nature of this improvement is not very clear yet, it is most probably related to the assembly process of clay–(Hb/PSS)$_n$ nanoclusters. The clay nanoparticles may have better adsorption selectivity toward Hb than toward the macromolecular impurities originally existing in Hb solution. Several cycles of washing/centrifugation/discarding steps may also help to remove the impurities from the nanoclusters. Thus, the assembly of clay–(Hb/PSS)$_n$ nanoclusters would also act as a purification process, and the purified Hb at the film electrodes would demonstrate better reversibility, as reported in literature [44,45]. The formal potential ($E^{o\prime}$) values of different Hb-containing clay films were similar but not exactly the same (Table 1), suggesting that the different film-making methods may make the microenvironment of clay films slightly different for Hb.

CVs of clay–(Hb/PSS)$_n$ films showed a strong dependence on pH of external buffers. Both reduction and oxidation peak potentials for clay–(Hb/PSS)$_n$ films shifted negatively with an increase in pH, while the peak shapes kept nearly unchanged. Take clay–(Hb/PSS)$_2$ films as an example. The formal potential ($E^{o\prime}$) estimated as the midpoint of reduction and oxidation CV peak potentials for Hb Fe(III)/Fe(II) redox couples showed a linear dependence on pH in the range of pH 5.0 to 12.0 with a slope of $-51.2$ mV pH$^{-1}$. This slope value is reasonably close to the theoretical value of $-58$ mV pH$^{-1}$ at 20 °C for a proton-coupled, reversible electrode process with equal numbers of protons and electrons transferred [46,47]. Hb has four subunits, each of which contains one heme prosthetic group. Thus, the electron transfer between Hb and PG electrodes in clay–(Hb/PSS)$_2$ films can be represented as $\mathrm{HemeFe(III)}+\mathrm{H^+}+\mathrm{e^-}\Leftrightarrow\mathrm{HemeFe(II)}$. An inflection point was observed at pH 5.0 in the $E^{o\prime}$–pH plot, and when pH <5.0, the variation of $E^{o\prime}$ with pH showed a much smaller slope of $-33.5$ mV pH$^{-1}$. The break in the $E^{o\prime}$–pH plot suggests that the protonatable site of amino acids near the heme region of Hb associated with the electrode reaction has an apparent p$K_a$ value of 5.0 [48,49]. Clay–(Hb/PSS) films showed the similar pH-dependent behavior.

Changes of CV peak potentials with pH were reversible. For example, a clay–(Hb/PSS)$_2$ film electrode was first placed in pH 5.0 buffers and tested by CV. It was then transferred to pH 7.0 buffers and examined by CV. When the film electrode was placed back into the pH 5.0 buffers again, the CV was quite reproducible and demonstrated almost the same peak potentials and heights as before.

To explain the reason why the fractions of electroactive Hb in clay–(Hb/PSS)$_n$ films were relatively small, the influence of film thickness was investigated. Taking clay–(Hb/PSS)$_2$ films as an example, various volumes of clay–(Hb/PSS)$_2$ dispersions with the same concentration of clay–(Hb/PSS)$_2$ were deposited on the PG electrodes to form clay–(Hb/PSS)$_2$ films with different film thickness, and CVs were performed to obtain the values of $\Gamma^*$. Results showed that while the $\Gamma^*$ value increased with the film thickness, the fraction of electroactive Hb decreases drastically (Table 2). This implies that only those Hb molecules in the inner layers of the films closest to the electrode surface are electrochemically addressable.

### 3.3. Stability and structure features

Long-term stability is one of the most important properties required for biosensors or bioreactors. The stability of clay–(Hb/PSS)$_n$ films modified on PG electrodes was tested by CV with two different methods. In solution studies, PG electrodes modified with clay–(Hb/PSS)$_n$ films were stored in pH 7.0 blank buffers during the whole storage time and CV tests were carried out periodically. Alternatively, with the "dry" method, clay–(Hb/PSS)$_n$ film electrodes were stored in air for most of the storage time and put into buffers occasionally for CV measurements. With both methods, clay–(Hb/PSS)$_n$ film electrodes showed excellent stability. The CV peak potentials kept in the same positions and the peak currents remained essentially unchanged for at least 40 days.

The Soret band of Hb was also used to monitor the stability of clay–(Hb/PSS)$_n$ films on quartz slides by UV–VIS spectroscopy. Clay–(Hb/PSS)$_n$ films cast on quartz slides were stored in pH 7.0 buffers and UV–VIS spectra were recorded periodically for the dry films after the slides were taken out of the solution and dried. The results showed that after 71 h of storage, the position of Soret band of dry clay–(Hb/PSS)$_n$ films at 412 nm was not changed, and the intensity of the UV–VIS peak maintained almost the same as its initial value.

The SEM top view of clay–(Hb/PSS)$_2$ films showed a lamellar flake-like structure with a lot of holes or cavities of different sizes (Fig. 2). Porous clay–(Hb/PSS)$_n$ films may absorb quite amounts of water when placed in solution and

Table 2
Dependence of the fraction of electroactive Hb on the deposited volume of clay–(Hb/PSS)$_2$ dispersion

| $V$/(μL) | $\Gamma$/(mol cm$^{-2}$) | $\Gamma^*$/(mol cm$^{-2}$) | $\Gamma^*/\Gamma$ |
|---|---|---|---|
| 2 | $5.4\times10^{-10}$ | $8.9\times10^{-11}$ | 16% |
| 5 | $1.4\times10^{-9}$ | $1.1\times10^{-10}$ | 7.8% |
| 10 | $2.7\times10^{-9}$ | $1.1\times10^{-10}$ | 4.2% |
| 15 | $4.0\times10^{-9}$ | $1.2\times10^{-10}$ | 3.0% |
| 20 | $5.4\times10^{-9}$ | $1.2\times10^{-10}$ | 2.3% |

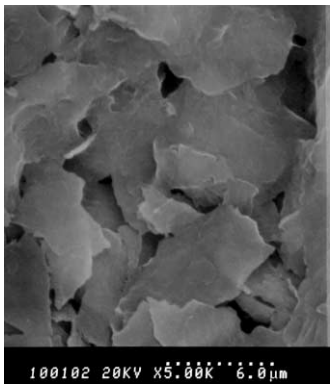


Fig. 2. SEM top view for clay–(Hb/PSS)$_2$ films cast on PG surface.

provide an aqueous-like microenvironment for the proteins, which may be favorable for Hb to exchange electrons with underlying PG electrodes. The porous films may also make small inorganic ions in buffers move into or out of the films more easily, which may greatly enhance the conductivity of the films and reduce the resistance of the charge transfer.

The peak of lowest reflection angle $2\theta$ of X-ray diffraction (XRD) for clay and clay–(Hb/PSS)$_n$ films was used to estimate the interlayer basal plane spacing of the films through Bragg's law [35]. A $2\theta$ peak was observed at 6.42° for clay films, showing a basal plane spacing of 13.8 Å (Fig. 3a). For clay–(Hb/PSS) and clay–(Hb/PSS)$_2$ films, the XRD peaks observed at 2.56° and 1.58° (Fig. 3b and c) showed larger basal plane spacing of 34.5 Å and 55.9 Å, respectively, indicating that Hb/PSS bilayers are intercalated into the clay layers and enlarge the interlayer spacing of the clay layers. XRD data of clay and clay–(Hb/PSS)$_n$ films are also listed in Table 3 for comparison.

The observation of Bragg's peak for XRD of clay and clay–(Hb/PSS)$_n$ films suggests a partially ordered layer structure in the films. The clay films cast from aqueous dispersions gave a basal plane spacing of 13.8 Å, larger than the value of 10.2 Å for clay films cast from organic solvent [50]. This was probably caused by water intercalation

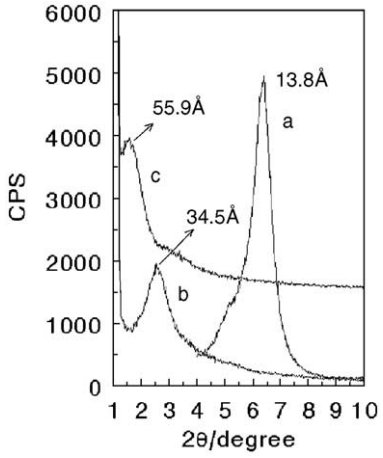


Fig. 3. X-ray diffraction patterns for (a) clay, (b) clay–(Hb/PSS), and (c) clay–(Hb/PSS)$_2$ films.

Table 3
X-ray diffraction results for clay and clay–(Hb/PSS)$_n$ films

| Films | $2\theta$ (°) | Basal plane spacing (Å) | Corrected interlayer spacing (Å) |
|---|---|---|---|
| Clay (from organic solvent) [50] | 8.66 | 10.2 | – |
| Clay (from aqueous dispersion) | 6.42 | 13.8 | – |
| Clay–(Hb/PSS) | 2.56 | 34.5 | 24.3 |
| Clay–(Hb/PSS)$_2$ | 1.58 | 55.9 | 45.7 |

between the clay layers in the former situation [23]. The value of 10.2 Å was thus used here as the thickness of dry clay platelets for a reference (Table 3). As expected, the net or corrected basal plane spacing of clay–(Hb/PSS)$_2$ films (45.7 Å) was about twice larger than clay–(Hb/PSS) films (24.3 Å). However, considering the size of Hb ($65 \times 55 \times 50$ Å [51]), it is difficult to explain why the corrected basal plane spacing of clay–(Hb/PSS) films was only about a half of the Hb dimension. It is probably related to the different properties of basal and edge planes of clay. While the basal plane of clay is always negatively charged, the edge plane of clay may become positively charged at suitable pH [52,53]. Some Hb/PSS bilayers adsorbed on clay surface may be rearranged during the drying process of the nanocluster films, in which the Hb surrounded by polyanionic PSS are probably arranged on the edge of clay platelets, thus enlarging the clay basal spacing by less than the dimension of Hb.

### 3.4. Conformational studies

Infrared spectra of proteins can provide information on the secondary structure of the proteins immobilized on solid surfaces [54,55]. For proteins, amide I band at 1700–1600 cm$^{-1}$ is caused by C=O stretching vibrations of the peptide linkage, and amide II band at 1600–1500 cm$^{-1}$ is caused by a combination of N–H in-plane bending and C–N stretching of the peptide groups. These two amide bands are sensitive markers for protein conformation changes. Reflective absorption infrared (RAIR) spectroscopy was used to characterize Hb in the core–shell clay–(Hb/PSS)$_n$ nanoclusters (Fig. 4A). The second derivative IR spectra can provide more detailed information on protein conformation than the original IR spectra. Negative second derivative bands are resolved from overlapped amide I and II bands in the original spectra, and frequencies have been assigned for α-helix, β-sheet, turns, disordered features and other secondary structural features of proteins [55]. The second derivative IR spectra were thus also presented to enhance the IR resolution (Fig. 4B). Pure Hb films demonstrated an IR peak at 1655 cm$^{-1}$ for amide I band, and a smaller one at 1542 cm$^{-1}$ for amide II band. For clay–(Hb/PSS)$_n$ films, amide I band was at 1657 cm$^{-1}$ for $n=1$ and 1655 cm$^{-1}$ for $n=2$, whereas amide II bands were at 1542 cm$^{-1}$ ($n=1$) and 1539 cm$^{-1}$ ($n=2$), respectively. Both amide bands of clay–(Hb/PSS)$_n$ films showed the

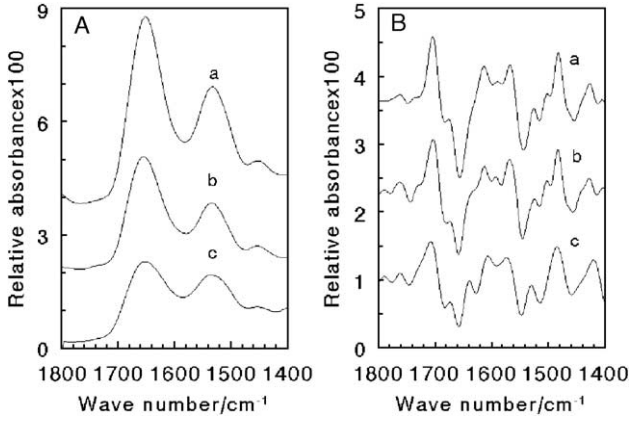


Fig. 4. (A) Original and (B) second-derivative microscopic RAIR spectra for (a) clay–(Hb/PSS)$_2$, (b) clay–(Hb/PSS), and (c) Hb films.

negative peak positions of the second-derivative IR spectra very similar to those of the pure Hb films, respectively. In addition, the second derivative IR spectra of clay–(Hb/PSS)$_n$ and pure Hb films demonstrated nearly identical patterns or curve shapes in most parts of the spectra. While the IR spectra at this resolution may not be good enough to provide complete information about the folded state of the protein, especially that of the quaternary structure of Hb, the present data support the speculation that the major portion of Hb essentially retains its native structure in the clay–(Hb/PSS)$_n$ films.

The shape and position of Soret absorption band of the heme prosthetic group in heme proteins may provide information on the possible denaturation of the proteins. Although the wavelength of Soret band may not be a sufficient diagnostic criterion for the conformational variation of the whole protein, it is relatively sensitive to the conformational change in the heme region [56,57]. UV–VIS spectroscopy was used to monitor the position change of the Soret band of Hb in clay–(Hb/PSS)$_n$ films (Fig. 5A). Both dry Hb and clay–(Hb/PSS)$_n$ films demonstrated Soret bands at 412 nm. When clay–(Hb/PSS)$_2$ films cast on quartz slides were placed into buffers at pH between 5.5 and 9.0, the Soret band was observed at 410 nm, very close to that at 412 nm for the dry Hb films. The results suggest that Hb in clay–(Hb/PSS)$_n$ film retain its near-native conformation in both dry form and "wet" form in the medium pH range. When pH was changed toward more acidic or more basic direction, the Soret band showed a blue-shift and became broader, indicating that Hb in clay–(Hb/PSS)$_n$ films may undergo denaturation to a considerable extent.

Hemin is the free heme group without polypeptide around it. As a control, the hemin and clay–(hemin/PSS) nanocluster films were also prepared on quartz slides and tested by UV–VIS spectroscopy. The spectra of both hemin and clay–(hemin/PSS) films displayed the Soret band at the wavelength less than 400 nm with much broader peak shapes (Fig. 5B), obviously different from that of dry Hb and clay–(Hb/PSS)$_2$ films (412 nm). In the aqueous solution, the Soret band of hemin also showed the blue-shift of peak position and broadening of peak shape compared with Hb (Fig. 5B), very similar to the situation in the film phase. UV–VIS results indicate that the heme group in Hb is not split out of the protein matrix in the nanocluster preparation.

To further investigate the possibility of release of the heme groups from Hb polypeptide matrix in the preparation of clay–(Hb/PSS)$_n$ nanocluster films, CVs of clay–(hemin/PSS) and clay–(catalase/PSS) films cast on PG electrodes were conducted (Fig. 6). Catalase is also a kind of heme proteins with MW of 240,000 and four similar subunits, each of which contains a heme group. The clay–(catalase/PSS) nanocluster films were prepared in the same way as the corresponding Hb films. While the CV response of clay–(catalase/PSS) films was very small, the direct and nearly reversible electrochemistry of catalase was obviously observed, and the peak potentials at around −0.48 V was believed to be attributed to catalase heme Fe(III)/Fe(II) redox couples [58]. To make the CVs of two protein films comparable in the same figure, a smaller amount of clay–(Hb/PSS) nanoclusters was cast on the PG surface. The results showed that while the midpoint peak potential of clay–(Hb/PSS) films (−0.36 V) was similar to that of clay–(hemin/PSS) films (−0.37 V), the average peak potential of clay–(catalase/PSS) films (−0.48 V) was more negative than that of clay–(hemin/PSS) films. If catalase in the nanocluster films were denatured and most of the heme groups in catalase were split out of the polypeptide matrix, the CV should have shown the obvious positive shift in peak potentials. Since the preparation methods for both Hb and catalase nanocluster films were the same, we speculate that the heme groups of Hb were also kept inside the polypeptide pockets and not released from the protein matrix in clay–(Hb/PSS)$_n$ films.

The results of both IR and UV–VIS spectroscopic experiments (Figs. 4 and 5), combined with that of the

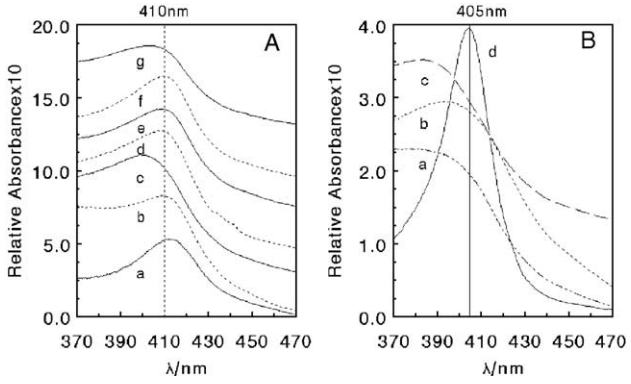


Fig. 5. (A) UV–VIS spectra on quartz slides for (a) dry Hb films, (b) dry clay–(Hb/PSS)$_2$ films, and clay–(Hb/PSS)$_2$ films in different pH buffers: (c) pH 2.5, (d) pH 5.5, (e) pH 7.0, (f) pH 9.0, (g) pH 12.0. (B) UV–VIS spectra of (a) clay–(hemin/PSS) films, (b) hemin films, and (c) $1.75\times10^{-6}$ M hemin, (d) $2.9\times10^{-7}$ M Hb in pH 7.0 buffers.

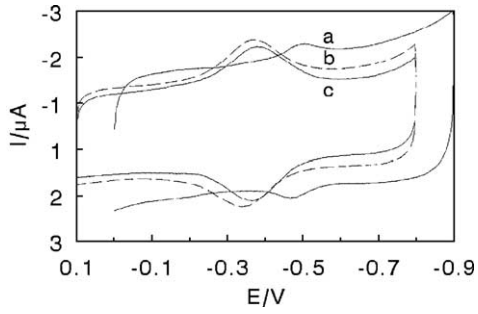


Fig. 6. Cyclic voltammograms at 0.2 V $s^{-1}$ in pH 7.0 buffers for (a) clay–(catalase/PSS), (b) clay–(Hb/PSS), and (c) clay–(hemin/PSS) films.

additional CVs (Fig. 6), support the conclusion that Hb retains its near-native structure in clay–$(Hb/PSS)_n$ films.

### 3.5. Electrochemical catalysis

Electrocatalytic activity of clay–$(Hb/PSS)_n$ films toward various substrates of biological or environmental significance was characterized by CV. For example, when a certain volume of air was injected into a pH 7.0 oxygen-free buffer through a syringe, a significant increase of CV reduction peak at about −0.35 V was observed at clay–$(Hb/PSS)_2$ film electrodes (Fig. 7d) compared with that in the absence of oxygen (Fig. 7c). The increase in reduction peak was accompanied by the disappearance of oxidation peak of HbFe(II), which had reacted with oxygen. An increase in the amount of injected air in solution resulted in an increase in reduction peak (Fig. 7e). For clay films without Hb, the direct reduction of oxygen was observed at about −0.85 V (Fig. 7b), far more negative than the catalytic reduction peak potential. Thus, the clay–$(Hb/PSS)_2$ film electrode lowered the reduction overpotential of $O_2$ by about 0.5 V. The catalytic efficiency, expressed as the ratio of reduction peak current in the presence ($I_c$) and absence of oxygen ($I_d$), $I_c/I_d$, decreased with an increase of scan rate, also characteristic of electrocatalytic reduction of oxygen by clay–$(Hb/PSS)_n$ films [59].

The electrocatalytic reduction of hydrogen peroxide at clay–$(Hb/PSS)_n$ film electrodes was also observed with CV.

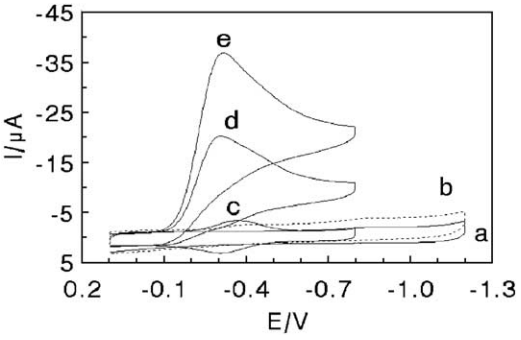


Fig. 7. Cyclic voltammograms at 0.2 V $s^{-1}$ in 10 mL of pH 7.0 buffers for (a) clay films, (b) clay films with 40 mL of air injected, (c) clay–$(Hb/PSS)_2$ films, (d) clay–$(Hb/PSS)_2$ films with 40 mL of air injected, and (e) clay–$(Hb/PSS)_2$ films with 80 mL of air injected.

Table 4
Catalytic performances of clay–$(Hb/PSS)_n$ films toward various substrates in pH 7.0 buffers

| Substrates | | Films | |
|---|---|---|---|
| | | Clay–(Hb/PSS) | Clay–$(Hb/PSS)_2$ |
| $O_2$[a] | Catalytic efficiency ($I_c/I_d$) | 3.3 | 3.8 |
| $H_2O_2$[b] (CV) | Catalytic efficiency ($I_c/I_d$) | 4.3 | 2.9 |
| | Linear range (mM) | 0.001–0.18 | 0.001–0.14 |
| | Detection limit (μM) | 1.0 | 1.0 |
| | Sensitivity (mA $M^{-1}$) | 84.2 | 85.4 |
| | Correlative coefficient | 0.999 | 0.997 |
| $H_2O_2$[c] | Response time (s) | 7 | 7 |
| (amperometry) | Linear range (mM) | 0.01–0.17 | 0.01–0.20 |
| | Sensitivity (mA $M^{-1}$) | 469 | 194 |
| | Correlation coefficient | 0.998 | 0.998 |
| $NaNO_2$[d] | Linear range (mM) | 0.04–3.6 | 0.04–4.0 |
| | Detection limit (mM) | 0.04 | 0.04 |
| | Sensitivity (mA $M^{-1}$) | 2.58 | 1.94 |
| | Correlative coefficient | 0.996 | 0.997 |

[a] CV, 0.2 V $s^{-1}$ 40 mL of air injected in 10 mL.
[b] 0.2 V $s^{-1}$.
[c] At constant potential of 0 V in pH 7.0 buffers.
[d] CV, 0.2 V $s^{-1}$.

When $H_2O_2$ was added to a pH 7.0 buffer, compared with the system with no $H_2O_2$ present, a significant increase in reduction peak at about −0.35 V was observed with the disappearance of oxidation peak for HbFe(II). The reduction peak current increased with the concentration of $H_2O_2$ in solution. The direct reduction of $H_2O_2$ at clay film electrodes was not observed. The catalytic CV reduction peak of clay–$(Hb/PSS)_n$ films showed a linear relationship with $H_2O_2$ concentration in certain range (Table 4). At higher $H_2O_2$ concentrations, the CV response showed a level-off tendency.

The electrocatalytic reduction of hydrogen peroxide at clay–$(Hb/PSS)_n$ film electrodes was also studied by amperometry. In the experiments, the potential was set at 0 V vs. SCE and the catalytic reduction currents were monitored when aliquots of $H_2O_2$ were added. At clay film electrode, no current increase was observed after addition of $H_2O_2$ (Fig. 8a). In contrast, with clay–$(Hb/PSS)_n$ films, a

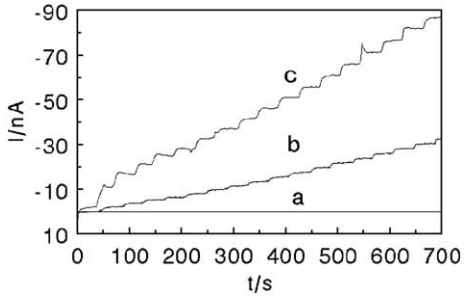


Fig. 8. Amperometric current–time curves at constant potential of 0 V vs. SCE in pH 7.0 buffers with injection of $H_2O_2$ every 40 s for (a) clay, (b) clay–$(Hb/PSS)_2$, and (c) clay–(Hb/PSS) films. Concentration increase of each step corresponds to 0.01 mM $H_2O_2$ for clay and clay–$(Hb/PSS)_n$ films.

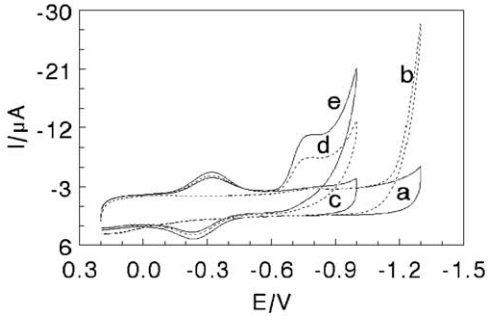


Fig. 9. Cyclic voltammograms at 0.2 V $s^{-1}$ in pH 5.5 buffers for (a) clay film, (b) clay film with 1.6 mM $NO_2^-$, (c) clay–$(Hb/PSS)_2$ film, (d) clay–$(Hb/PSS)_2$ film with 1.6 mM $NO_2^-$, and (e) clay–$(Hb/PSS)_2$ film with 3.2 mM $NO_2^-$.

stepped increase of $H_2O_2$ concentration in buffer solutions caused the corresponding growth of reduction currents (Fig. 8b and c). The current had a linear relationship with concentration of $H_2O_2$ in solution. The catalytic performance of clay–(Hb/PSS) and clay–$(Hb/PSS)_2$ films toward hydrogen peroxide is also listed in Table 4 for comparison.

Catalytic reduction of nitrite was also studied at clay–$(Hb/PSS)_n$ film electrodes. For example, with clay–$(Hb/PSS)_2$ films, a new reduction wave appeared at about −0.75 V when $NO_2^-$ was added in pH 5.5 buffers (Fig. 9). The wave height increased with a further addition of $NO_2^-$. Direct reduction of $NO_2^-$ on clay film with no Hb present was found at the potential more negative than −1.2 V. Thus, the clay–$(Hb/PSS)_2$ film decreased the reduction overpotential of $NO_2^-$ by at least 0.4 V. The catalytic CV reduction peak of the clay–$(Hb/PSS)_n$ films had a linear relationship with $NO_2^-$ concentration in a certain range (Table 4).

The catalytic performances of clay–$(Hb/PSS)_n$ films toward different substrates are summarized in Table 4. For the substrates of oxygen, clay–$(Hb/PSS)_2$ films with $n=2$ showed better catalytic efficiency ($I_c/I_d$) than clay–(Hb/PSS) films with $n=1$. For $H_2O_2$ and $NO_2^-$ systems, however, clay–(Hb/PSS) films seem to be more active than clay–$(Hb/PSS)_2$ films in catalysis. For instance, for the catalytic reduction of $H_2O_2$ with CV, clay–(Hb/PSS) films demonstrated much higher catalytic efficiency ($I_c/I_d$) than clay–$(Hb/PSS)_2$ films. In the meantime, the former displayed better sensitivity than the latter in the determination of $H_2O_2$ by amperometry, qualitatively consistent with the results of CV. The biocatalytic activity of Hb in these core–shell nanocluster films toward different substrates could thus be more precisely tailored by controlling the number of bilayers of the shells.

There are only a few quantitative data available for other Hb-containing clay films in catalysis, it is thus difficult to make a systematic comparison of clay–$(Hb/PSS)_n$ films with other Hb-containing clay films in electrocatalysis of various substrates. Nevertheless, some comparisons of the Hb nanocluster films with the cast Hb–clay films [32] could be made. The clay–$(Hb/PSS)_n$ films demonstrated better CV catalytic efficiency toward both oxygen and hydrogen peroxide than the Hb–clay films. As for comparison with other cast Hb films, such as Hb–polyelectrolyte films, clay–$(Hb/PSS)_n$ films displayed electrocatalytic activity generally at the same level without showing obvious advantages. However, some improvements were also observed toward certain substrates for the nanocluster films if compared with some specific Hb films. For example, clay–$(Hb/PSS)_n$ films demonstrated lower detection limit in determination of nitrite than that of most other cast Hb films, such as Hb-PAMAM [60] and Hb-CMC [61] films, where PAMAM is polyamidoamine dendrimer and CMC is carboxymethyl cellulose.

## 4. Conclusion

The stable and ordered clay–$(Hb/PSS)_n$ nanocluster films provide a favorable microenvironment for Hb to transfer electrons with underlying PG electrodes. The construction strategy of this core–shell structure provides a controllable route to immobilize proteins and improves the electrochemical reversibility of the proteins at their nanocluster film electrodes. Hb can retain its near-native secondary structure in clay–$(Hb/PSS)_n$ films, and exhibit good electrocatalytic activity toward various substrates with biological or environmental significance. The electrochemical and electrocatalytic activity of the films can be tailored by controlling the number of bilayers of the $(Hb/PSS)_n$ shells on the surface of clay nanoparticle cores and by adjusting the film thickness of the films. This new type of protein core–shell nanocluster films might have potential applicability in constructing biosensors or bioreactors based on the direct electrochemistry of enzyme without using any mediator.

## Acknowledgements

Financial support from the National Natural Science Foundation of China (NSFC 20275006 and 20475008) is greatly acknowledged.

## References

[1] F.M. Chaplin, C. Bucke, Enzyme Technology, Cambridge University Press, Cambridge, 1990.
[2] F.A. Armstrong, G.S. Wilson, Recent developments in faradaic bioelectrochemistry, Electrochim. Acta 45 (2000) 2623–2645.
[3] J.F. Rusling, Z. Zhang, in: R.W. Nalwa (Ed.), Handbook of Surfaces and Interfaces of Materials, vol. 5, Academic Press, New York, 2001, p. 33.
[4] N. Hu, Direct electrochemistry of redox proteins or enzymes at various film electrodes and their possible applications in monitoring some pollutants, Pure Appl. Chem. 73 (2001) 1979–1991.
[5] J.F. Rusling, Enzyme bioelectrochemistry in cast biomembrane-like films, Acc. Chem. Res. 31 (1998) 363–369.

[6] F.A. Armstrong, H.A.O. Hill, N.J. Walton, Direct electrochemistry of redox proteins, Acc. Chem. Res. 21 (1988) 407–413.
[7] Y. Lvov, in: Y. Lvov, H. Mohwald (Eds.), Protein Architecture: Interfacing Molecular Assemblies and Immobilization Biotechnology, Marcel Dekker, New York, 2000, p. 125.
[8] J.F. Rusling, in: Y. Lvov, H. Mohwald (Eds.), Protein Architecture: Interfacing Molecular Assemblies and Immobilization Biotechnology, Marcel Dekker, New York, 2000, p. 337.
[9] Y. Lvov, Z. Lu, J. Schenkman, X. Zu, J.F. Rusling, Direct electrochemistry of myoglobin and cytochrome $P450_{cam}$ in alternate layer-by-layer films with DNA and other polyions, J. Am. Chem. Soc. 120 (1998) 4073–4080.
[10] H. Ma, N. Hu, J.F. Rusling, Electroactive myoglobin films grown layer-by-layer with poly(styrenesulfonate) on pyrolytic graphite electrodes, Langmuir 16 (2000) 4969–4975.
[11] L. Wang, N. Hu, Direct electrochemistry of hemoglobin in layer-by-layer films with poly(vinyl sulfonate) grown on pyrolytic graphite electrodes, Bioelectrochemistry 53 (2001) 205–212.
[12] P. He, N. Hu, G. Zhou, Assembly of electroactive layer-by-layer films of hemoglobin and polycationic poly(diallyldimethylammonium), Biomacromolecules 3 (2002) 139–146.
[13] Z. Li, N. Hu, Assembly of electroactive layer-by-layer films of myoglobin and ionomer poly(ester sulfonic acid), J. Colloid Interface Sci. 254 (2002) 257–265.
[14] P. He, N. Hu, J.F. Rusling, Driving forces for layer-by-layer self-assembly of films of $SiO_2$ nanoparticles and heme proteins, Langmuir 20 (2004) 722–729.
[15] P. He, N. Hu, Electrocatalytic properties of heme proteins in layer-by-layer films assembled with $SiO_2$ nanoparticles, Electroanalysis 16 (2004) 1122–1131.
[16] P. He, N. Hu, Interactions between heme proteins and Dextran sulfate in layer-by-layer assembly films, J. Phys. Chem., B 108 (2004) 13144–13152.
[17] F. Caruso, H. Mohwald, Protein multilayer formation on colloids through a stepwise self-assembly technique, J. Am. Chem. Soc. 121 (1999) 6039–6046.
[18] F. Caruso, C. Schuler, Enzyme multilayers on colloid particles: assembly, stability, and enzymatic activity, Langmuir 16 (2000) 9595–9603.
[19] Y. Lvov, F. Caruso, Biocolloids with ordered urease multilayer shells as enzymatic reactors, Anal. Chem. 73 (2001) 4212–4217.
[20] H. Sun, N. Hu, Voltammetric studies of hemoglobin-coated polystyrene latex bead films on pyrolytic graphite electrodes, Biophys. Chemist. 110 (2004) 297–308.
[21] H. Sun, N. Hu, Electroactive layer-by-layer films of heme protein-coated polystyrene latex beads with poly(styrenesulfonate), Analyst 130 (2005) 76–84.
[22] H. Liu, N. Hu, Electroactive core–shell nanocluster films of heme proteins, polyelectrolytes, and silica nanoparticles, Langmuir 20 (2004) 10700–10705.
[23] A.J. Bard, T. Mallouk, in: R.W. Murray (Ed.), Molecular Design of Electrode Surface, Wiley, New York, 1992, p. 159.
[24] C. Fan, Y. Zhuang, G. Li, J. Zhu, D. Zhu, Direct electrochemistry and enhanced catalytic activity for hemoglobin in a sodium montmorillonite film, Electroanalysis 12 (2000) 1156–1158.
[25] C. Lei, U. Wollenberger, N. Bistolas, A. Guiseppi-Elie, F.W. Scheller, Electron transfer of hemoglobin at electrodes modified with colloidal clay nanoparticles, Anal. Bioanal. Chem. 372 (2002) 235–239.
[26] X. Chen, N. Hu, Y. Zeng, J.F. Rusling, J. Yang, Ordered electrochemically active films of hemoglobin, didodecyldimethylammonium ions, and clay, Langmuir 15 (1999) 7022–7030.
[27] C. Lei, F. Lisdat, U. Wollenberger, F.W. Scheller, Cytochrome *c*/clay-modified electrode, Electroanalysis 111 (1999) 274–276.
[28] Y. Sallez, P. Bianco, E. Lojou, Electrochemical behavior of c-type cytochromes at clay-modified carbon electrodes: a model for the interaction between proteins and soils, J. Electroanal. Chem. 493 (2000) 37–49.
[29] C. Lei, U. Wollenberger, C. Jung, F.W. Scheller, Clay-bridged electron transfer between cytochrome $P450_{cam}$ and electrode, Biochem. Biophys. Res. Commun. 268 (2000) 740–744.
[30] V. Shumyantseva, Y.D. Ivanov, N. Bistolas, F.W. Scheller, A.I. Archakov, U. Wollenberger, Direct electron transfer of cytochrome P450 2B4 at electrodes modified with nonionic detergent and colloidal clay nanoparticles, Anal. Chem. 76 (2004) 6046–6052.
[31] S. Kroning, F.W. Scheller, U. Wollenberger, F. Lisdat, Myoglobin-clay electrode for nitric oxide (NO) detection in solution, Electroanalysis 16 (2004) 253–259.
[32] Y. Zhou, N. Hu, Y. Zeng, J.F. Rusling, Heme protein–clay films: direct electrochemistry and electrochemical catalysis, Langmuir 18 (2002) 211–219.
[33] Z. Li, N. Hu, Direct electrochemistry of heme proteins in their layer-by-layer films with clay nanoparticles, J. Electroanal. Chem. 558 (2003) 155–165.
[34] Y. Zhou, Z. Li, N. Hu, Y. Zeng, J.F. Rusling, Layer-by-layer assembly of ultrathin films of hemoglobin and clay nanoparticles with electrochemical and catalytic activity, Langmuir 18 (2002) 8573–8579.
[35] C. Shi, J.F. Rusling, Z. Wang, W.S. Winiecki, A.M. Winiecki, S.L. Suib, Electrocatalytic reactions in organized assemblies: 6. Electrochemical and spectroscopic studies of catalytic clay micelle electrodes, Langmuir 5 (1989) 650–660.
[36] J.B. Matthew, G.I.H. Hanania, F.R.N. Gurd, Electrostatic effects in hemoglobin–hydrogen-ion equilibria in human deoxyhemoglobin and oxyhemoglobin-A, Biochemistry 18 (1979) 1919–1928.
[37] Q. Huang, Z. Lu, J.F. Rusling, Composite films of surfactants, Nafion, and proteins with electrochemical and enzyme activity, Langmuir 12 (1996) 5472–5480.
[38] R.W. Murray, in: A.J. Bard (Ed.), Electroanalytical Chemistry, vol. 13, Marcel Dekker, New York, 1986, p. 191.
[39] A.J. Bard, L.R. Faulkner, Electrochemical Methods, Wiley, New York, 1980.
[40] J.G. Osteryoung, J.J. O'Dea, in: A.J. Bard (Ed.), Electroanalytical Chemistry, vol. 14, Marcel Dekker, New York, 1986, pp. 209–308.
[41] J.J. O'Dea, J.G. Osteryoung, Characterization of quasi-reversible surface processes by square-wave voltammetry, Anal. Chem. 65 (1993) 3090–3097.
[42] Z. Zhang, J.F. Rusling, Electron transfer between myoglobin and electrodes in thin films of phosphatidylcholines and dihexadecylphosphate, Biophys. Chemist. 63 (1997) 133–146.
[43] A.-E.F. Nassar, Z. Zhang, N. Hu, J.F. Rusling, T.F. Kumosinski, Proton-coupled electron transfer from electrodes to myoglobin in ordered biomembrane-like films, J. Phys. Chem., B 101 (1997) 2224–2231.
[44] T. Daido, T. Akaike, Electrochemistry of cytochrome *c*: influence of coulombic attraction with indium tin oxide electrode, J. Electroanal. Chem. 344 (1993) 91–106.
[45] I. Taniguchi, K. Watanabe, M. Tominaga, F.M. Hawkridge, Direct electron transfer of horse heart myoglobin at an indium oxide electrode, J. Electroanal. Chem. 333 (1992) 331–338.
[46] L. Meites, Polarographic Techniques, 2nd ed., Wiley, New York, 1965.
[47] A.M. Bond, Modern Polarographic Methods in Analytical Chemistry, Marcel Dekker, New York, 1980.
[48] D. Bashford, D.A. Case, C. Dalvit, L. Tennant, P.E. Wright, Electrostatic calculations of side-chain $pK_a$ values in myoglobin and comparison with NMR data for histidines, Biochemistry 32 (1993) 8045–8056.
[49] A.-S. Yang, B. Honig, Structural origins of pH and ionic-strength effects on protein stability: acid denaturation of sperm whale apomyoglobin, J. Mol. Biol. 237 (1994) 602–614.
[50] J.F. Rusling, M.F. Ahmadi, N. Hu, Surfactant-intercalated clay films containing metal phthalocyanines, Langmuir 8 (1992) 2455–2460.
[51] M.F. Perutz, H. Muirhead, J.M. Cox, L.C.G. Goaman, F.S. Mathews, E.L. McGandy, L.E. Webb, 3-Dimensional Fourier synthesis of horse

oxyhaemoglobin at 2.8 a resolution—(I) X-ray analysis, Nature 219 (1968) 131–139.
[52] G. Lagaly, S. Ziesmer, Colloid chemistry of clay minerals: the coagulation of montmorillonite dispersions, Adv. Colloid Interface Sci. 100–102 (2003) 105–128.
[53] A.K. Bajpai, R. Sachdeva, Study on the adsorption of hemoglobin onto bentonite clay surfaces, J. Appl. Polym. Sci. 85 (2002) 1607–1618.
[54] H. Torii, M. Tasumi, in: H.H. Mantsch, D. Chapman (Eds.), Infrared Spectroscopy of Biomolecules, Wiley, New York, 1996, p. 1.
[55] J.F. Rusling, T.F. Kumosinski, Nonlinear Computer Modeling of Chemical and Biochemical Data, Academic Press, New York, 1996, pp. 117–134.
[56] H. Theorell, A. Ehrenberg, Spectrophotometric, magnetic, and titrimetric studies on the heme-linked groups in myoglobi, Acta Chem. Scand. 5 (1951) 823–848.
[57] P. George, G. Hanania, Spectrophotometric study of ionizations in methemoglobin, J. Biochem. 55 (1953) 236–243.
[58] Z. Zhang, S. Chouchane, R.S. Magliozzo, J.F. Rusling, Direct voltammetry and catalysis with *Mycobacterium tuberculosis* catalase-peroxidase, peroxidases, and catalase in lipid films, Anal. Chem. 74 (2002) 163–170.
[59] C.P. Andrienx, C. Blocman, J.M. Dumas-Bouchiat, F. M'Halla, J.M. Saveant, Homogeneous redox catalysis of electrochemical reactions: Part V. Cyclic voltammetry, J. Electroanal. Chem. 113 (1980) 19–40.
[60] L. Shen, N. Hu, Heme protein films with polyamidoamine dendrimer: direct electrochemistry and electrocatalysis, Biochim. Biophys. Acta, Bioenerg. 1608 (2004) 23–33.
[61] H. Huang, P. He, N. Hu, Y. Zeng, Electrochemical and electrocatalytic properties of myoglobin and hemoglobin incorporated in carboxymethyl cellulose films, Bioelectrochemistry 61 (2003) 29–38.